ChemPubSoc Europe

DOI: 10.1002/celc.201300104

Electrochemical Cycling of Sodium-Filled Silicon Clathrate

Nicholas A. Wagner,[a] Rahul Raghavan,[a] Ran Zhao,[b] Qun Wei,[c, d] Xihong Peng,[c] and Candace K. Chan*[a]

Due to their high charge-storage capacity (i.e. $>3000\ mA\,h\,g^{-1}$), there has been much research activity in the development of silicon-based anodes for high-energy-density lithium-ion batteries. In recent years, there has been immense interest in understanding the electrochemical,[1,2] structural,[3–5] and mechanical properties[6–8] of both diamond cubic (c-Si) and amorphous silicon (a-Si) under reaction with lithium. Silicon with a clathrate or cage-like structure has been recently investigated as a potential anode, with both theoretical[9] and experimental verification by Langer et al.[10] that lithiation is feasible. Since prior studies on silicon clathrates have focused predominately on their superconducting[11–18] and thermoelectric[19–24] properties, this is a potentially new and exciting application for this class of materials. Type-I clathrates of the form M_8Si_{46}, where M is a guest atom intercalated into the structure, are made of two pentagonal dodecahedra (Si_{20}) cages and six tetrakaidecahedra (Si_{24} cages) per unit cell and crystallize in the $Pm\bar{3}n$ space group (Figure 1 a). Type-II clathrates[25] of the form M_xSi_{136} ($0<x<24$), are made of sixteen pentagonal dodecahedra plus eight hexakaidecahedra (Si_{28} cages) per unit cell and crystallize in the $Fd\bar{3}m$ space group (Figure 1 b). Detailed X-ray diffraction (XRD) and nuclear magnetic resonance (NMR) studies of the lithiation process into practically guest free type-II clathrate $Na_{1.3}Si_{136}$[10] showed that the clathrate structure could be maintained until insertion of 24 Li per formula unit. Upon insertion of more Li, the clathrate structure became amorphous and eventually transformed into crystalline $Li_{15}Si_4$ (c-$Li_{15}Si_4$), much like is observed during lithiation of c-Si. However, no delithiation behavior was shown in this previous work, and no extended cycling data were shown. To this end, we have conducted an extended electrochemical, structural, and theoretical study of sodium-filled silicon clathrate to better understand its properties as an anode for lithium-ion batteries.

Sodium-filled silicon clathrate was synthesized from the decomposition of Zintl phase NaSi.[26–28] XRD patterns of the as-

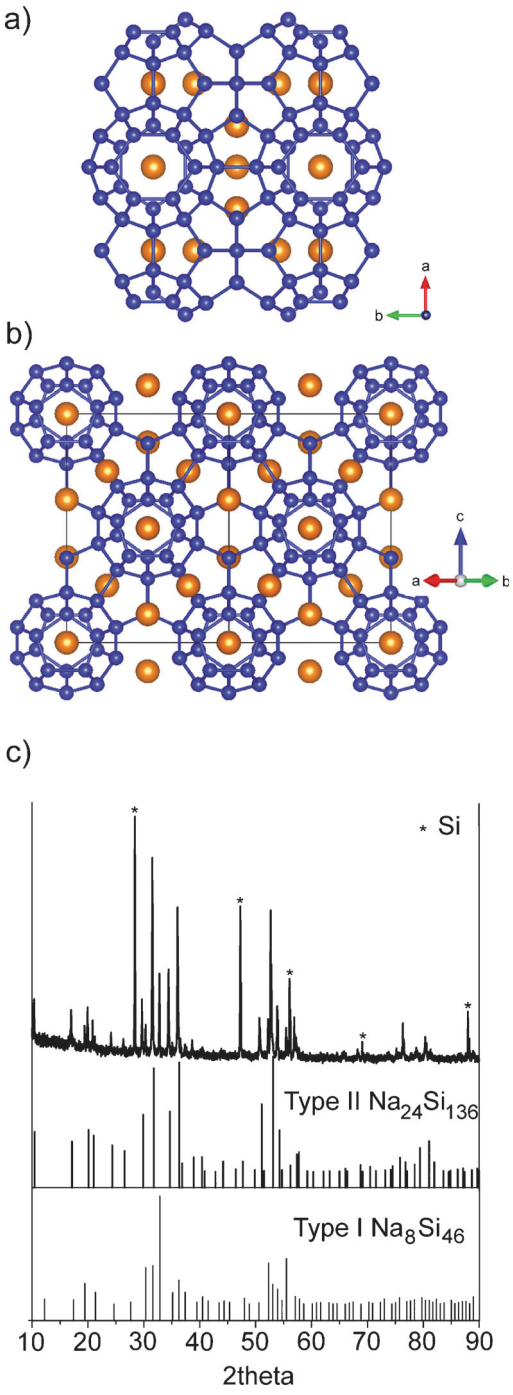

Figure 1. a) Structure of type-I clathrate Na_8Si_{46}. b) Structure of type-II $Na_{24}Si_{136}$ clathrate. c) XRD of the as-made product. The peaks from c-Si are marked with asterisks.

[a] *N. A. Wagner, R. Raghavan, Prof. C. K. Chan*
Materials Science and Engineering
School for Engineering of Matter, Transport and Energy
Arizona State University, Tempe, AZ 85287 (USA)
E-mail: candace.chan@asu.edu

[b] *R. Zhao*
Department of Chemistry and Biochemistry
Arizona State University, Tempe, AZ 85287 (USA)

[c] *Dr. Q. Wei, Prof. X. Peng*
School of Letters and Sciences
Arizona State University, Mesa, AZ 85212 (USA)

[d] *Dr. Q. Wei*
School of Science, Xidian University, Xi'an, 710071 (PR China)

Supporting information for this article is available on the WWW under http://dx.doi.org/10.1002/celc.201300104.

 © 2014 Wiley-VCH Verlag GmbH & Co. KGaA, Weinheim

made samples showed that the product was a mixture of both type-I and type-II clathrate, as well as c-Si. The presence of c-Si in the product may be due to evaporation loss of Na during the synthesis, which has been counteracted through addition of excess Na in other reports.[28,29] Although Horie et al.[29] observed pure-phase type-II clathrate at decomposition temperatures below 440 °C, we obtained a mixture of products using similar conditions. Figure 1c shows the powder XRD pattern of the as-made product along with reference patterns for Na_8Si_{46}[26] and $Na_{24}Si_{136}$[30] from the literature. After treatment with NaOH, the c-Si peaks were absent from the XRD pattern (Figure S1, Supporting Information), leaving only the peaks from the clathrates. The phase fraction, as determined by Rietveld analysis, showed that the powder was composed of about 80% type-II clathrate and 20% type-I clathrate.

Scanning electron microscopy (SEM) imaging revealed that the particles were approximately 1–5 μm in diameter (Figure S2a). Energy-dispersive X-ray spectroscopy (EDS) analysis showed an average composition of 14.4 at% Na and 85.6 at% Si, with a standard deviation of 3.2%. This corresponds to a Na:Si ratio of 0.169, which is in close agreement with the ratios in Na_8Si_{46} and $Na_{24}Si_{136}$, suggesting that the Na sites in the clathrates were almost fully occupied. The powders were mixed into slurries with carbon black and polyvinylidene difluoride (PVDF) binder, then coated onto Cu foil. SEM images of the coated films showed that the carbon black formed a conducting network around the clathrate particles (Figure S2b).

Potentiodynamic cycling of the clathrate films was performed to understand the basic electrochemical processes occurring in the electrodes during lithium insertion (charge) and de-insertion (discharge) in half-cells with Li metal counter electrodes. The cycling results using a 25 μA mg^{-1} threshold current are shown in Figure 2a. The first charge was characterized by a flat plateau at around 0.120 V (vs. Li/Li$^+$), similar to the plateau observed during lithiation of c-Si.[1] However, since the XRD patterns showed that c-Si was etched away, and no features consistent with lithiation of a-Si were observed, these electrochemical features are likely from the reaction of Li with the clathrates. The discharge curve showed a flat plateau at 0.425 V and had a similar shape to that observed in the delithiation of c-$Li_{15}Si_4$,[1] although at a slightly lower voltage. The first charge capacity was 2431 mA h g^{-1}, and the discharge capacity was 1213 mA h g^{-1}, resulting in a Coulombic efficiency (CE) of about 50% (Figure 2b). A prior study on lithiation of $Na_{1.3}Si_{136}$ by Langer et al.[10] did not report any discharge curves, and the lithiation capacities presented in that work were only 1300–1600 mA h g^{-1}. Our results show that discharge of lithiated clathrate is possible, although subsequent cycling revealed drastic decreases in capacity to about 171 mA h g^{-1} at the fifth cycle. The charge profiles also became sloped starting with the second cycle, although the discharge profiles remained flat. The low CE, even at the fifth cycle (only about 80%), could be due to pulverization from phase transformations or volume changes, since similar CE are observed in micron-sized Si particles[31] whereas nanostructured Si anodes,[32,33] which do not pulverize, show much higher CE.

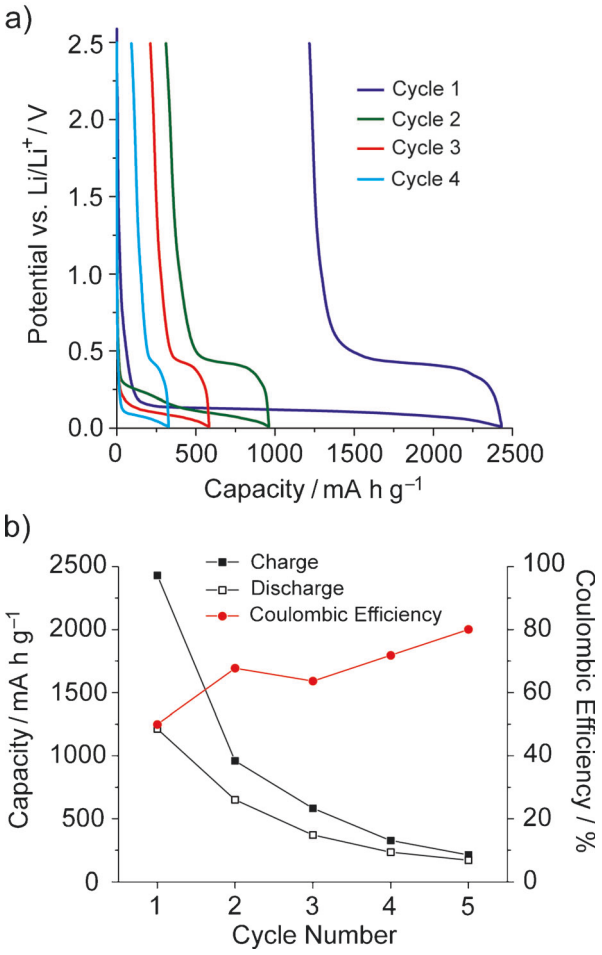

Figure 2. a) Voltage versus capacity determined by potentiodynamic cycling with a 25 μA mg^{-1} threshold current. b) Capacity and Coulombic efficiency.

On the other hand, such low CE could also be due to poorly passivated surfaces and solid electrolyte interphase (SEI) formation, which is not yet understood for silicon bonded in the clathrate structure.

To better understand the lithiation and delithiation features of Na-filled silicon clathrate, differential charge (dQ) versus potential plots were obtained for this system and compared to the results obtained for c-Si. Figures 3a and 3b show the first and second cycles, respectively, for an electrode cycled using a 25 μA mg^{-1} threshold current. Due to the differences in the observed capacities, the values of the dQ were scaled to clearly distinguish the differences between the two materials. The absolute, un-scaled plots for the clathrates are shown in Figure S3. Overall, the dQ plots of the clathrates look very similar to those for c-Si. Lithiation of c-Si is characterized by a transformation to amorphous Li_xSi in a two-phase reaction in the first charge, followed by conversion to c-$Li_{15}Si_4$ at voltages below 50 mV (vs. Li/Li$^+$).[1] Delithiation of c-$Li_{15}Si_4$ occurs as a two-phase reaction to form amorphous Si (a-Si) at the end of the discharge. These two-phase reactions are observed as peaks in the dQ versus potential plots.

The similar shape of the dQ plots for the clathrates suggests a similar reaction mechanism. Prior XRD and NMR analyses

© 2014 Wiley-VCH Verlag GmbH & Co. KGaA, Weinheim

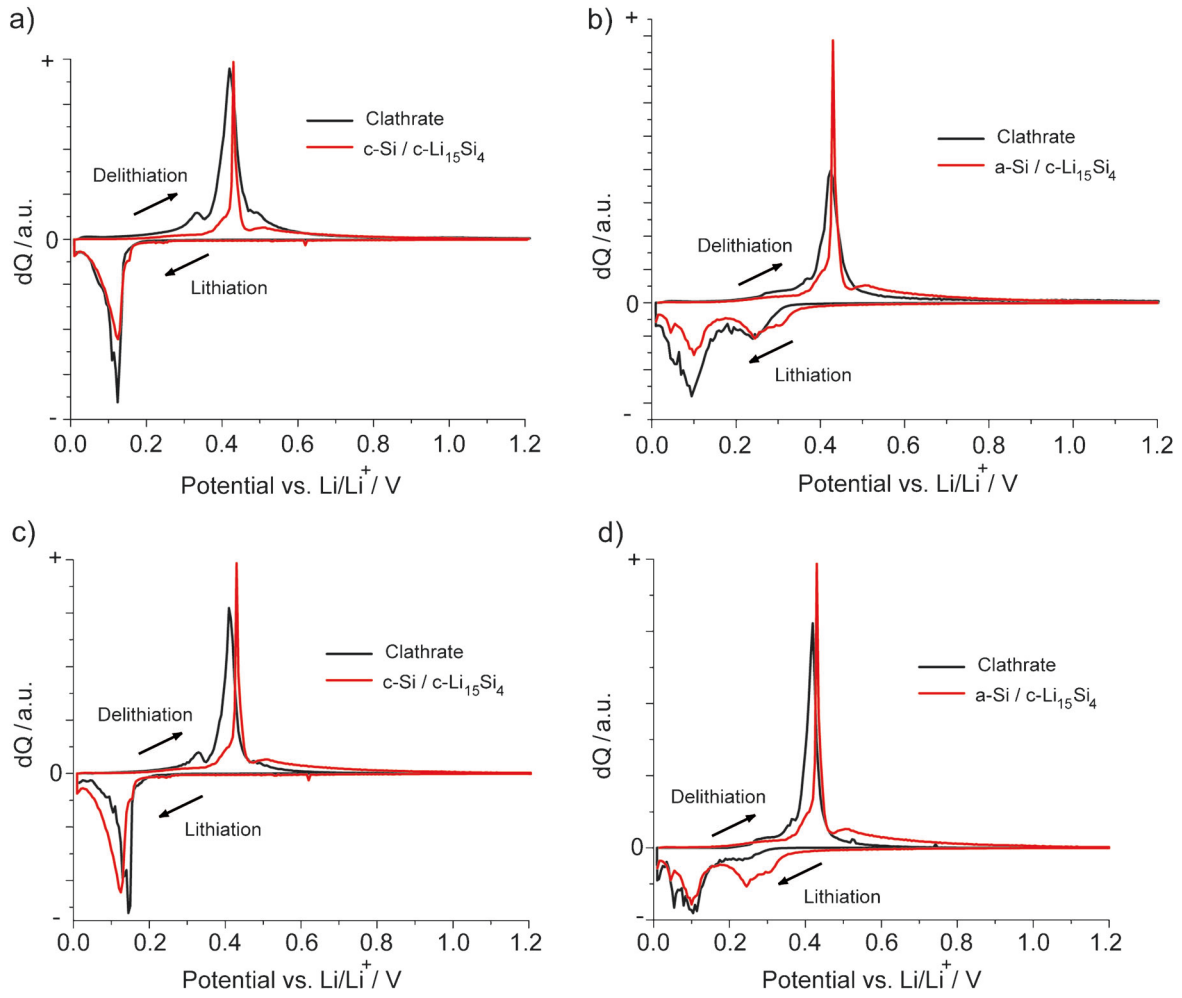

Figure 3. Differential charge plots of clathrate compared to c-Si and a-Si using a 25 $\mu A\,mg^{-1}$ (a,b) and a 5 $\mu A\,mg^{-1}$ (c,d) threshold current. (a) and (c) are the first cycle and (b) and (d) are the second cycle. The values of the differential charge were scaled to facilitate comparison.

showing an amorphization and formation of c-$Li_{15}Si_4$ upon lithiation of $Na_{1.3}Si_{136}$[10] are consistent with these observations. Another key difference between the clathrate d*Q* plots and those for delithiation of c-$Li_{15}Si_4$ is that the discharge was observed over a broader range of potentials for the clathrate. There is also a notable peak at 0.3 V (vs. Li/Li^+) in the discharge, which is not seen in delithiation of c-$Li_{15}Si_4$. The second charge of the clathrate (Figure 3b) showed two broad peaks, which are similar to those seen in lithiation of a-Si, although at slightly lower potentials. When performing cycling with a 5 $\mu A\,mg^{-1}$ threshold current (Figure 3c–Figure 3d), the voltage hysteresis between the charge and discharge decreased from 0.28 V when using 25 $\mu A\,mg^{-1}$ to 0.25 V, but the other features remained largely the same.

In the results reported by Langer,[10] a plateau at 0.3 V (vs. Li/Li^+) was observed in the initial stage of the charge, with a capacity of about 100 $mA\,h\,g^{-1}$. Since in their work the starting clathrate material was $Na_{1.3}Si_{134}$, this feature was attributed to the insertion of about 24 Li per unit cell of type-II clathrate to form $Li_{24}Si_{136}$. Insertion of more Li was found to result in a lower reaction potential of about 0.25 V, which corresponded to the amorphization of the material in a similar process as what occurs in c-Si. However, the charge curve was notably sloped, suggesting a single-phase reaction mechanism. We did not observe this 0.3 V lithiation feature in our case and our lithiation potentials were much lower and not sloped in the first charge. This can possibly be explained by the fact that our type-II clathrate has a higher occupancy by Na, which can decrease the observed voltage and change the reaction mechanism in the first charge to a two-phase reaction. We also have a larger fraction of type-I clathrate in our sample, but currently it is unclear what role the Na_8Si_{46} clathrate plays in the observed electrochemical characteristics.

To confirm the amorphization process, ex situ XRD measurements were performed on the cells after galvanostatic cycling using a current of 25 $\mu A\,mg^{-1}$. The peaks attributed to the unlithiated clathrate (Figure 4a) were observed to decrease in intensity after lithiation to about 1300 $mA\,h\,g^{-1}$ (Figure 4b), confirming the amorphization process. This capacity corresponds to about 184 Li inserted into the clathrate (or ~1.6 Li/Si), assuming a composite anode of type-I and type-II clathrate with a total molecular weight of approximately 3790 $g\,mol^{-1}$, based

© 2014 Wiley-VCH Verlag GmbH & Co. KGaA, Weinheim

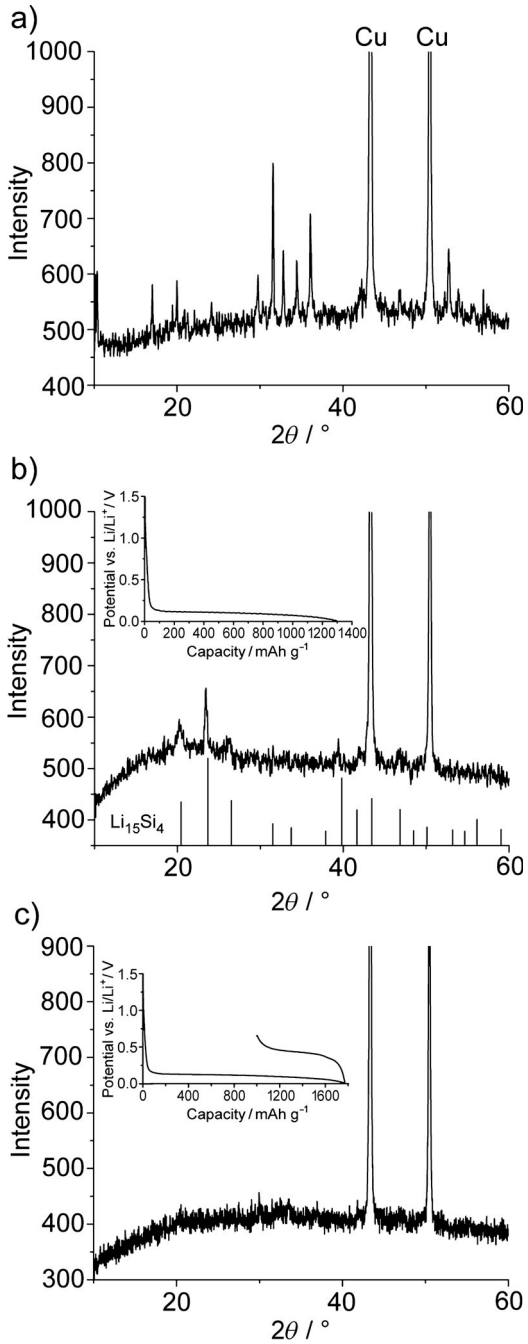

Figure 4. XRD patterns of clathrate films on Cu: a) prior to cycling, b) after lithiation, and c) after lithiation and delithiation. The insets in (b) and (c) show the corresponding galvanostatic cycling curves.

on the phase fraction obtained from the Rietveld analysis. Several reflections corresponding to c-$Li_{15}Si_4$ were also observed (Figure 4b).

For a sample that was lithiated to 1770 mA h g^{-1} and then partially discharged, the c-$Li_{15}Si_4$ peaks disappeared and no new reflections were observed (Figure 4c), indicating that the material transformed into an amorphous phase during delithiation of c-$Li_{15}Si_4$. These results are consistent with the observed electrochemical characteristics. SEM imaging of the samples after ten cycles showed that the clathrate particles were covered with an SEI layer, but no obvious pulverization or cracks were observed in the particles (Figure S2c–d).

To better understand the amorphization process, first-principles density functional theory (DFT) was applied to calculate the lattice constant and energy of formation for several structures using the Vienna Ab initio Simulations Package (VASP) code.[34,35] The results for Si_{136}, $Na_{24}Si_{136}$, Na_8Si_{46}, $Li_{24}Si_{136}$, $Li_{16}Na_{24}Si_{136}$, and $Li_{15}Si_4$ are shown in Table 1. Although the calculated formation energies for Na_8Si_{46} and empty Si_{136} were slightly positive, both structures have been experimentally synthesized. Note that the calculated formation energies are based on the total energies predicted by DFT at the ground state, that is, 0 K, so the calculated values are reasonable. The formation energy for fully filled $Na_{24}Si_{136}$ was −0.005 eV per atom, suggesting it is the more stable structure compared to empty Si_{136}.

Table 1. Calculated properties, determined by DFT.

Compound	Lattice constant [Å]	Formation energy [eV per atom]
Si_{136}	14.74	0.052
Na_8Si_{46}	10.24	0.002
$Na_{24}Si_{136}$	14.78	−0.005
$Li_{24}Si_{136}$	14.68	0.030
$Li_{16}Na_{24}Si_{136}$	14.95	0.012
$Li_{16}Na_{24}Si_{136}'$	14.90	−0.002
$Li_{16}Na_{24}Si_{136}''$	14.90	−0.003
$Li_{15}Si_4$	10.54	−0.239

To model lithiated clathrate, the type-II structure was considered since our synthesized powders were predominately this phase. Type-II clathrate crystallizes in the $Fd\bar{3}m$ space group, with Si occupying the 8a, 32e, and 96 g sites and Na in the 8b and 16c sites, as described with Wyckoff symmetry notation. Replacing the Na with Li to form $Li_{24}Si_{136}$ resulted in a formation energy of 0.030 eV per atom, which is higher than that for $Na_{24}Si_{136}$. This is likely due to the ability of Na to better stabilize the clathrate structure due to its larger size. Despite this slightly positive formation energy, electrochemical Li insertion into the empty Na sites of type-II clathrate has been confirmed by NMR,[10] as previously described.

Lithiation of Na-filled type-II clathrate was first modeled by placing Li into the 16d sites, which are typically unoccupied in type-II clathrate, to form $Li_{16}Na_{24}Si_{136}$ (Figure 5a). The Si_{28} polyhedra in type-II clathrate are composed of 12 pentagonal and four hexagonal faces. Occupancy of the 16d sites by Li places them on the faces of the hexagons, equidistant from each Si, such that they are bisected and shared by neighboring Si_{28} clusters (Figure 5b). In this configuration, the Li species are located in channels along the <110> directions parallel to the rows of Na ions occupying the 16c sites. The Li–Si and Na–Li bond lengths were 2.454 and 3.237 Å, respectively, in this structure. The formation energy for this structure was 0.012 eV per atom, lower than that for $Li_{24}Si_{136}$. These results suggest that lithiation into Na-filled clathrate is not less favorable than lithiation into empty clathrate.

© 2014 Wiley-VCH Verlag GmbH & Co. KGaA, Weinheim

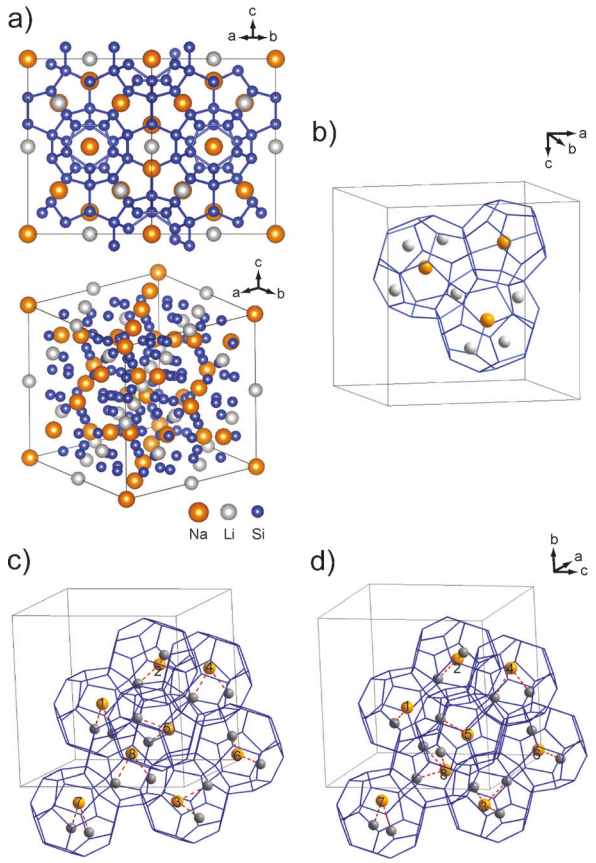

Figure 5. Structures of $Li_{16}Na_{24}Si_{136}$ calculated by DFT: a,b) $Li_{16}Na_{24}Si_{136}$ with Li in the 16d sites. b) Unit cell for $Li_{16}Na_{24}Si_{136}$ showing the arrangement of Li atoms on the hexagon faces separating the Si_{28} cages. Several cages were deleted for clarity. c) Unit cell for $Li_{16}Na_{24}Si_{136}'$ and d) $Li_{16}Na_{24}Si_{136}''$ showing all eight Si_{28} cages. The Si_{20} cages were deleted for clarity. The Na atoms are labeled and the Na–Li bonds are indicated by red dashed lines.

Next, the positions of the Li species were displaced slightly from the 16d sites so that they were no longer sitting in the hexagonal faces, but rather inside the Si polyhedra. In the first structure, which we call $Li_{16}Na_{24}Si_{136}'$, two Li atoms were placed inside the Si_{28} cages so that they shared the interstitial space with the Na atoms (Figure 5c). The second structure, which we call $Li_{16}Na_{24}Si_{136}''$, had the Li atoms distributed amongst the eight Si_{28} cages of the unit cell in the following manner: two cages had one Li, two cages had three Li, and the remaining four cages had two Li sharing the cage volume with the Na (Figure 5d). The calculated Na atomic coordinates for both structures showed that the Na positions were shifted away from the centers of the cages to accommodate the Li atoms. Both structures had negative formation energies (Table 1) and shorter bond lengths than in the original $Li_{16}Na_{24}Si_{136}$ structure, with the shortest bond length of 2.837 Å calculated in $Li_{16}Na_{24}Si_{136}''$ (Table S1).

Importantly, these results suggest that it is energetically feasibly for more than one guest atom to occupy the space inside the Si_{28} cage of type-II clathrate while maintaining the overall Si clathrate framework structure. The lattice constants for all of the lithiated type-II clathrate structures increased very slightly compared to the empty Si_{136}. This suggests that at the initial stages of Li insertion, the clathrate structure may be maintained. However, with more Li insertion, the experimental results show that transformation into an amorphous lithium and sodium containing silicide is more favorable. The formation energy of c-$Li_{15}Si_4$ was calculated to be −0.239 eV per atom. The very low energy for this phase can explain why lithiation of both empty[10] and Na-filled (this work) clathrate eventually result in transformation to c-$Li_{15}Si_4$.

In summary, electrochemical and XRD analyses of lithium insertion into a mixture of Na-filled type-I and type-II clathrates showed a similar reaction mechanism in these materials as is found in diamond cubic silicon. Upon electrochemical lithiation, the clathrates became amorphous and transformed into c-$Li_{15}Si_4$ at low potentials, then remained an amorphous silicide after delithiation. The low Coulombic efficiencies and poor capacity retention observed are likely due to pulverization from the phase transformation and volume changes during lithiation of the amorphous silicide, which is also typically observed in micron-sized Si particles. However, low CE from poorly passivating SEI layers cannot be ruled out, and this will be investigated further in future studies. DFT was applied to calculate the lattice constants and formation energies for various type-II clathrate structures. The results showed that 16 Li atoms could be inserted per unit cell with very little increase in lattice constant. The DFT-predicted structures for $Li_{16}Na_{24}Si_{136}$ containing multiple-guest atoms inside the larger Si_{28} cages shows that these configurations are energetically favorable and suggests that such lithiation processes can occur without significant changes in lattice constant or clathrate structure. Future work will focus on understanding the phase transformations in the clathrate structures during the initial stages of lithiation. The formation of clathrate structures with multiple guest atoms within the same cage may also yield materials with interesting and novel electronic properties for other applications.

Experimental Section

Synthesis

The synthesis of Na-filled clathrate was performed by thermal decomposition of the Zintl compound NaSi.[26–28] NaSi was purchased from SiGNa Chemistry and dried at 100 °C to remove adsorbed moisture. NaSi was loaded into a h-BN crucible, then placed in a quartz tube and heated in a tube furnace under continuous vacuum evacuation (~10^{-4} Torr). The sample was heated to 340 °C (ramp rate of 10.5 °C min^{-1}) and held for 30 min, then ramped using the same rate to 420 °C and held for 18 h. After 18 h, the furnace was turned off while the sample remained under continuous vacuum for 6 h to remove Na vapor and enable the formation of more type-II clathrate.[28] After the synthesis, the powder was quenched successively with toluene, isopropanol, ethanol, and water to remove any unreacted Na. To remove unreacted silicon, the powder was treated with 1 M NaOH for 8 h.

Characterization

Powder X-ray diffraction (XRD) was performed using CuKα radiation on a PANalytical X'Pert Pro diffractometer. Structure refine-

© 2014 Wiley-VCH Verlag GmbH & Co. KGaA, Weinheim

ment of the XRD data was performed using Bruker-AXS Topas 4.2. XRD patterns were indexed to structures for type-I and type-II clathrate from the literature.[26,30] XRD measurements on electrodes after electrochemical cycling were performed by washing the electrode with hexanes after cell disassembly. Peak positions and intensities were normalized to the reflections originating from the Cu foil substrate. Scanning electron microscopy (SEM) and energy-dispersive X-ray spectroscopy (EDS) were performed on a FEI XL30 ESEM-FEG. EDS was performed on 14 different particles to obtain an average composition.

Electrochemical Testing

Clathrate powder was mixed with carbon black (Timcal Super C45) and polyvinylidene difluoride (PVDF) in an 80:10:10 weight ratio and dissolved in N-methyl-2-pyrrolidone. This slurry was coated onto a copper foil with a Meyer rod and dried at 100 °C. The mass of the coating was determined using a microbalance (Mettler-Toledo, UMX2). Pouch cells were assembled in an Ar-filled glovebox using a Li metal foil as the counter electrode, a Celgard 3401 separator, and 1 M $LiPF_6$ in a 1:1 mixture of ethylene carbonate and diethylcarbonate (Novolyte). The cells were tested by potentiodynamic cycling to perform electrochemical potential spectroscopy[36] from 2–0.01 V (vs. Li/Li^+) with a 5 mV potential step amplitude and threshold current of either 5 or 25 $\mu A\,mg^{-1}$ based on the mass of the clathrate. For preparing samples for ex situ XRD analysis after lithiation and delithiation, galvanostatic testing using a 25 $\mu A\,mg^{-1}$ current density was performed.

Computational Methods

First-principles density functional theory (DFT) was applied to calculate the lattice constants and energies of the clathrate structures employing the VASP code.[34,35] The Perdew–Burke–Ernzerhof (PBE) functional[37] and projector-augmented wave (PAW)[37] potentials were used along with the plane-wave basis sets. The energy cutoff for the plane-wave basis set was 300 eV. The convergence criteria for energy and forces were set to be 0.01 and 0.1 meV respectively. The Si 3 s3p, Na 2p3 s, Li 1 s2 s electrons were treated as valence electrons. The formation energies were calculated by subtracting the total energies of the elements from the energy of the structure, then dividing by the total number of atoms. For example, the formation energy for Si_{136} was calculated using [Eq. (1)] and that for $Li_{16}Na_{24}Si_{136}$ was calculated using [Eq. (2)], where $E(Si), E(Li)$ and $E(Na)$ are the energies per atom for c-Si, Li and Na metals, respectively:

$$E_{\text{form}} = \frac{E(Si_{136}) - 136E(Si)}{136} \quad (1)$$

$$E_{\text{form}} = \frac{E(Li_{16}Na_{24}Si_{136}) - 16E(Li) - 24E(Na) - 136E(Si)}{176} \quad (2)$$

Acknowledgements

This work was carried out using new faculty startup funds from the Fulton Schools of Engineering (C.K.C.), Faculty Scholarship Support from the School of Letters and Sciences (X.P.), and support from the National Science Foundation (DMR-1206795). N.A.W. would like to thank the Fulton Undergraduate Research Initiative at ASU for funding. The authors gratefully acknowledge the use of facilities within the LeRoy Eyring Center for Solid State Science at ASU and thank D. Wright for assistance with the clathrate synthesis and E. Soignard and D. Mieritz for assistance with structure refinement. We also acknowledge the ASU Advanced Computing Center for providing computational resources on the Saguaro Cluster.

Keywords: anodes · clathrate · energy storage · lithium-ion batteries · silicon

[1] M. N. Obrovac, L. Christensen, *Electrochem. Solid-State Lett.* **2004**, *7*, A93 – A96.
[2] C. K. Chan, R. Ruffo, S. S. Hong, R. A. Huggins, Y. Cui, *J. Power Sources* **2009**, *189*, 34 – 39.
[3] T. D. Hatchard, J. R. Dahn, *J. Electrochem. Soc.* **2004**, *151*, A838 – A842.
[4] J. Li, J. R. Dahn, *J. Electrochem. Soc.* **2007**, *154*, A156 – A161.
[5] B. Key, R. Bhattacharyya, M. Morcrette, V. Seznec, J.-M. Tarascon, C. P. Grey, *J. Am. Chem. Soc.* **2009**, *131*, 9239.
[6] S. W. Lee, M. T. McDowell, L. A. Berla, W. D. Nix, Y. Cui, *Proc. Natl. Acad. Sci. USA* **2012**, *109*, 4080.
[7] H. L. Liu, H. Zheng, L. Zhong, S. Huang, K. Karki, L. Q. Zhang, Y. Liu, A. Kushima, W. T. Liang, J. W. Wang, J.-H. Cho, E. Epstein, S. A. Dayeh, S. T. Picraux, T. Zhu, J. Li, J. P. Sullivan, J. Cummings, C. Wang, S. X. Mao, Z. Z. Ye, S. Zhang, J. Y. Huang, *Nano Lett.* **2011**, *11*, 3312.
[8] X. H. Liu, L. Zhong, S. Huang, S. X. Mao, T. Zhu, J. Y. Huang, *ACS Nano* **2012**, *6*, 1522.
[9] K. S. Chan, C. K. Chan, W. Liang, *United States Patent Application* No. 12/842, *224*, **2010**.
[10] T. Langer, S. Dupke, H. Trill, S. Passerini, H. Eckert, R. Pöttgen, W. Winter, *J. Electrochem. Soc.* **2012**, *159*, A1318 – A1322.
[11] H. Kawaji, H. Horie, S. Yamanaka, M. Ishikawa, *Phys. Rev. Lett.* **1995**, *74*, 1427 – 1429.
[12] F. Shimizu, Y. Maniwa, K. Kume, H. Kawaji, S. Yamanaka, M. Ishikawa, *Phys. Rev. B* **1996**, *54*, 13242 – 13246.
[13] R. F. W. Herrmann, K. Tanigaki, S. Kuroshima, H. Suematsu, *Chem. Phys. Lett.* **1998**, *283*, 29 – 32.
[14] S. Yamanaka, E. Enishi, H. Fukuoka, M. Yasukawa, *Inorg. Chem.* **2000**, *39*, 56 – 58.
[15] E. Reny, A. San-Miguel, Y. Guyot, B. Masenelli, P. Melinon, L. Saviot, S. Yamanaka, B. Champagnon, C. Cros, M. Pouchard, M. Borowski, A. J. Dianoux, *Phys. Rev. B* **2002**, *66*, 014532.
[16] H. Fukuoka, J. Kiyoto, S. Yamanaka, *Inorg. Chem.* **2003**, *42*, 2933 – 2937.
[17] D. Connetable, V. Timoshevskii, B. Masenelli, J. Beille, J. Marcus, B. Barbara, A. M. Saitta, G. Rignanese, P. Melinon, S. Yamanaka, X. Blase, *Phys. Rev. Lett.* **2003**, *91*, 247001.
[18] P. Toulemonde, C. Adessi, X. Blase, A. San Miguel, *Phys. Rev. B* **2005**, *71*, 094504.
[19] N. P. Blake, L. Mollnitz, G. Kresse, H. Metiu, *J. Chem. Phys.* **1999**, *111*, 3133 – 3144.
[20] G. S. Nolas, G. A. Slack, S. B. Schujman in *Semiconductors and Semimetals*, Vol. 69 (Ed.: T.M. Tritt), Elsevier, **2001**, *69*, 255 – 300.
[21] C. L. Condron, J. Martin, G. S. Nolas, P. M. B. Piccoli, A. J. Schultz, S. M. Kauzlarich, *Inorg. Chem.* **2006**, *45*, 9381 – 9386.
[22] M. Christensen, S. Johnsen, B. B. Iversen, *Dalton Trans.* **2010**, *39*, 978 – 992.
[23] N. Tsujii, J. H. Roudebush, A. Zevalkink, C. A. Cox-Uvarov, G. J. Snyder, S. M. Kauzlarich, *J. Solid State Chem.* **2011**, *184*, 1293-1303.
[24] S. Bobev, S. C. Sevov, *J. Solid State Chem.* **2000**, *152*, 92 – 105.
[25] A. San-Miguel, P. Toulemonde, *High Pressure Res.* **2005**, *25*, 159 – 185.
[26] G. K. Ramachandran, J. Dong, J. Diefenbacher, J. Gryko, R. F. Marzke, O. F. Sankey, P. F. McMillan, *J. Solid State Chem.* **1999**, *145*, 716 – 730.
[27] G. K. Ramachandran, J. Diefenbacher, O. F. Sankey, R. Sharma, R. F. Marzke, M. O'Keefe, J. Gryko, P. F. McMillan, *Mater. Res. Soc. Symp. Proc.* **1999**, *507*, 483 – 486.
[28] H. Horie, T. Kikudome, K. Teramura, S. Yamanaka, *J. Solid State Chem.* **2009**, *182*, 129 – 135.
[29] P. T. Hutchins, O. Leynaud, L. A. O'Dell, M. E. Smith, P. Barnes, P. F. McMillan, *Chem. Mater.* **2011**, *23*, 5160 – 5167.

© 2014 Wiley-VCH Verlag GmbH & Co. KGaA, Weinheim

[30] P. Melinon, P. Keghelian, A. Perez, B. Champagnon, Y. Guyot, L. Saviot, E. Reny, C. Cros, M. Pouchard, A. J. Dianoux, *Phys. Rev. B* **1999**, *59*, 10099.
[31] J. H. Ryu, J. W. Kim, Y.-E. Sung, S. M. Oh, *Electrochem. Solid-State Lett.* **2004**, *7*, A306 – A309.
[32] C. K. Chan, H. Peng, G. Liu, K. McIlwrath, X. F. Zhang, R. A. Huggins, Y. Cui, *Nat. Nanotechnol.* **2008**, *3*, 31 – 35.
[33] H. Wu, G. Chan, J. W. Choi, I. Ryu, Y. Yao, M. T. McDowell, S. W. Lee, A. Jackson, Y. Yang, L. Bing, Y. Cui, *Nat. Nanotechnol.* **2012**, *7*, 310.
[34] G. Kresse, J. Furthmuller, *Phys. Rev. B* **1996**, *54*, 11169.
[35] J. P. Perdew, K. Burke, M. Ernzerhof, *Phys. Rev. Lett.* **1996**, *77*, 3865.
[36] A. H. Thompson, *J. Electrochem. Soc.* **1979**, *126*, 608 – 616.
[37] G. Kresse, D. Joubert, *Phys. Rev. B* **1999**, *59*, 1758 – 1775.

Received: July 19, 2013
Published online on September 23, 2013

© 2014 Wiley-VCH Verlag GmbH & Co. KGaA, Weinheim